International Journal of Advance Research Publication and Reviews

Vol 03, Issue 10, pp 747-760, October, 2026

Ion-Beam-Driven Electrostatic Instability in a Magnetized, Relativistically Degenerate Plasma with Quantum Diffraction and Exchange–Correlation Effects

Iqbal Ahsan [1], Muhammad Rizwan[1], Shahnaz Maryam[2]*

[1]*Department of Physics, Government College University Faisalabad, Faisalabad, Pakistan*

[2]*Department of Information Technology, Bahauddin Zakariya University, Multan, Pakistan*

[*]*Email:* iqbalahsan4341@gmail.com

ABSTRACT

The linear stability of an ion beam streaming along a magnetic field through a dense plasma with relativistically degenerate electrons is investigated using a three-fluid quantum hydrodynamic model. Electrons obey the Chandrasekhar equation of state and include quantum diffraction (Bohm potential) and exchange–correlation effects, while the background ions and the beam are warm and magnetized and the waves propagate obliquely to the field. A closed dispersion relation is derived and reduced to a degree-eight polynomial whose complex roots yield the growth rate. Analytical limits are obtained for the quantum ion-acoustic mode, the two magnetized oblique modes, and a weak, cold beam. In the last case the growth rate scales as the cube root of the beam density, and the relevant wavenumber is the field-aligned component for a magnetized beam but the full wavenumber for an unmagnetized one. For a helium plasma at $n_{e0} = 10^{29}\ \mathrm{cm}^{-3}$, a beam density ratio of 0.1 and a beam speed of 1.6 times the quantum ion-acoustic speed, the maximum growth rate is $0.0615\,\omega_{pi}$, or $1.7 \times 10^{16}\ \mathrm{s}^{-1}$. Parallel propagation is unstable only for beam speeds between about 0.7 and 1.8 times the ion-acoustic speed, whereas oblique propagation extends the instability, with the largest growth at about 53°. Relativistic degeneracy is the dominant correction: the non-relativistic Fermi pressure overestimates the peak growth rate by 34% at $10^{29}\ \mathrm{cm}^{-3}$. Quantum diffraction and exchange–correlation change it by about 1% in the regime of validity of the fluid model. The results are relevant to white dwarf interiors and compressed inertial-fusion targets.

Keywords: Ion-beam Instability; Relativistic Degenerate Plasma; Chandrasekhar Equation of State; Quantum Hydrodynamics; Exchange–Correlation; Magnetized Plasma

1. Introduction

Plasmas in which the electron Fermi energy greatly exceeds the thermal energy are found in the interiors of white dwarfs and neutron-star envelopes, in warm dense matter, and in compressed inertial-confinement-fusion targets (Betti & Hurricane, 2016; Dornheim et al., 2018; Shukla & Eliasson, 2011). The recent achievement of target gain above unity in laser-driven fusion (Abu-Shawareb et al., 2024) has renewed interest in the collective dynamics of such degenerate plasmas. In compact stars the electron density can exceed $10^{30}\ \mathrm{cm}^{-3}$, so the Fermi momentum becomes comparable to $m_e c$ and the electron pressure follows the relativistic Chandrasekhar equation of state (Chandrasekhar, 1935). Many white dwarfs also carry strong magnetic fields (Ferrario et al., 2020; Schreiber et al., 2022).

Quantum hydrodynamic (QHD) models offer a tractable description of collective phenomena in such systems. They include the Fermi pressure, quantum diffraction through the Bohm potential, and, in extended versions, exchange–correlation effects (Haas et al., 2003; Manfredi & Haas, 2001; Shukla & Eliasson, 2012). The foundations and range of applicability of QHD have been examined critically by Moldabekov et al. (2018) and Bonitz et al. (2019). For relativistically degenerate electrons, Haas (2016) compared fluid and kinetic descriptions of ion-acoustic waves, and relativistic fluid models have been applied to ion-acoustic envelope modes (McKerr et al., 2016), weakly nonlinear excitations (Behery et al., 2016), shock waves (Atteya et al., 2017) and modulational instability (Abdikian, 2017). Related studies have treated nucleus-acoustic waves (Sultana & Schlickeiser, 2018), strongly coupled ions (Patidar & Sharma, 2020) and magnetized plasmas with arbitrary degeneracy (Haas & Mahmood, 2016).

Exchange–correlation effects have been incorporated through the local potential introduced by Brey et al. (1990) and applied to quantum plasmas by

Shukla & Eliasson (2012). Subsequent work examined their influence on multidimensional ion-acoustic waves (Roy & Sahu, 2020), on nonlinear ion-acoustic dynamics (Shome et al., 2020), and on magnetized quantum plasmas (Gul & Ahmad, 2021; Mahmood et al., 2019). Oblique propagation in magnetized dense plasmas has been analysed for ion-acoustic solitary and shock structures (El-Borie et al., 2020; Sultana et al., 2019) and in magneto-rotating quantum plasmas (Sahu et al., 2019), while Rajabi & Mohammadnejad (2023) studied modulational instability with a Fermi-gas equation of state.

Streaming instabilities are a central mechanism for converting the free energy of particle beams into wave energy. In quantum plasmas, two-stream and streaming instabilities have been studied in unmagnetized non-relativistic plasmas (Singh et al., 2022), in non-degenerate plasmas with quantum recoil (Lee & Jung, 2018), in spin-polarized electron–positron–ion plasmas (Khanum et al., 2020), and including quantum electrodynamic corrections (Bret, 2021). Ghai et al. (2019) showed that a neutrino beam can drive ion-acoustic waves unstable in an ultrarelativistic degenerate plasma. Ion beams in degenerate magnetoplasmas have been considered mainly for nonlinear structures: solitary waves in relativistic degenerate magnetoplasmas (Deka et al., 2018), hypersonic solitons with Landau degeneracy (Deka & Dev, 2018), shocks in weakly relativistic ion-beam magnetoplasmas (Kaur & Saini, 2021), and solitary waves with finite ion and beam temperatures (Madhukalya et al., 2023).

The closest linear study is that of Elkamash et al. (2017), who derived the dispersion relation of an unmagnetized, ultradense electron–ion plasma with an ion beam using a relativistic QHD model. They identified electron-plasma, ion-acoustic and beam-driven modes, and examined the dependence of the growth rate on beam density and speed. Their model, however, did not include a magnetic field, oblique propagation, exchange–correlation or finite ion and beam temperatures.

The present work extends this line of research in four respects. First, the background ions and the beam are magnetized and warm, and the wave vector is oblique to the field, so the problem becomes genuinely three-dimensional. Second, the electron response includes the full Chandrasekhar pressure together with the Bohm and exchange–correlation terms, which allows their relative importance to be quantified. Third, we derive analytical growth rates for a weak cold beam in both the magnetized and unmagnetized limits and verify them against exact roots. Fourth, we compare growth rates in physical units across densities at fixed beam speed, isolating the role of relativistic degeneracy.

The paper is organized as follows. Section 2 presents the model. Section 3 derives the dispersion relation, and Section 4 obtains its analytical limits. Numerical results are discussed in Section 5, and conclusions are given in Section 6.

2 Theoretical model

2.1 Plasma configuration

We consider a plasma of degenerate electrons (density n_e, charge $-e$, mass m_e), background ions (density n_i, charge Ze, mass m_i, temperature T_i) and an ion beam of the same species (density n_b, temperature T_b). The beam drifts with velocity $\mathbf{v}_{b0} = v_{b0}\hat{\mathbf{z}}$ along a uniform magnetic field $\mathbf{B}_0 = B_0\hat{\mathbf{z}}$. Electrostatic perturbations $\mathbf{E}_1 = -\nabla\phi_1$ propagate with wave vector $\mathbf{k} = k\sin\theta\,\hat{\mathbf{x}} + k\cos\theta\,\hat{\mathbf{z}}$, where θ is the angle to the field. Gaussian units are used. Equilibrium quasi-neutrality requires

$$n_{e0} = Z(n_{i0} + n_{b0}) = Zn_{i0}(1+\delta), \qquad \delta = \frac{n_{b0}}{n_{i0}}, \tag{1}$$

where δ is the beam-to-background density ratio. Since $\mathbf{v}_{b0} \parallel \mathbf{B}_0$, the equilibrium Lorentz force on the beam vanishes.

The model rests on three approximations, whose validity is quantified in Section 5. First, electron inertia is neglected, which requires the phase speed to be much smaller than the relativistic Fermi speed $v_{Fe} = cR/\sqrt{1+R^2}$; at the reference point the ratio is 0.012. Second, the electrostatic approximation requires the phase speed to lie below the Alfvén speed V_A. Here $v_{ph}/V_A \approx 0.34$, so electromagnetic corrections of relative order $\left(v_{ph}/V_A\right)^2 \approx 0.1$ may arise. Third, the magnetic field must be non-quantizing, $\hbar\omega_{ce} \ll \mu_e$, for the isotropic Chandrasekhar pressure to apply. Otherwise Landau quantization modifies the electron equation of state, as considered for ion-beam magnetoplasmas by Deka & Dev (2018) and Kaur & Saini (2021).

2.2 Electron dynamics

For waves whose phase speed is far below the electron Fermi speed, electron inertia can be neglected. The electron force balance is then (Manfredi & Haas, 2001; Shukla & Eliasson, 2011)

$$0 = en_e\nabla\phi - \frac{e}{c}\,n_e\mathbf{v}_e \times \mathbf{B}_0 - \nabla P_e + \frac{\hbar^2 n_e}{2m_e}\nabla\left(\frac{\nabla^2\sqrt{n_e}}{\sqrt{n_e}}\right) - n_e\nabla V_{xc}, \tag{2}$$

where the terms on the right represent the electrostatic force, the Lorentz force, the degeneracy pressure force, the quantum Bohm force and the exchange–correlation force. The component of Eq. (2) along $\hat{\mathbf{z}}$ eliminates the Lorentz force and, for $k_z \neq 0$, determines the electron density response.

The electron pressure is given by the Chandrasekhar equation of state (Chandrasekhar, 1935):

$$P_e = \frac{\pi m_e^4 c^5}{3h^3}\left[R(2R^2-3)\sqrt{1+R^2} + 3\sinh^{-1}R\right], \qquad R = \frac{p_F}{m_e c} = \frac{\hbar(3\pi^2 n_e)^{1/3}}{m_e c}, \tag{3}$$

where p_F is the Fermi momentum and R is the relativistic degeneracy parameter; $R = 1$ corresponds to $n_e \approx 5.9 \times 10^{29}$ cm^{-3}. Using the zero-temperature Gibbs–Duhem relation $dP_e = n_e\, d\mu_e$ with $\mu_e = m_e c^2\sqrt{1+R^2}$, the compressibility is

$$C_e^2 \equiv \frac{1}{m_e}\frac{dP_e}{dn_e} = \frac{c^2}{3}\frac{R^2}{\sqrt{1+R^2}}, \tag{4}$$

which reduces to $v_{Fe}^2/3$ for $R \ll 1$ and to $c^2 R/3 \propto n_e^{1/3}$ for $R \gg 1$ (Haas, 2016; McKerr et al., 2016). Relativity therefore softens the equation of state at high density.

The exchange–correlation potential is (Brey et al., 1990; Shukla & Eliasson, 2012)

$$V_{xc} = -0.985\, e^2 n_e^{1/3}\left[1 + \frac{0.034}{a_B n_e^{1/3}}\ln\left(1 + 18.37\, a_B n_e^{1/3}\right)\right], \tag{5}$$

where a_B is the Bohr radius. Its density derivative is negative, so the corresponding force opposes the degeneracy pressure. We measure its strength by

$$\alpha_{xc} = -\frac{n_{e0}}{m_e C_e^2}\frac{dV_{xc}}{dn_e} = \frac{0.985\, e^2}{3 m_e C_e^2 n_{e0}^{1/3}}\left[1 + \frac{0.034 \times 18.37}{1 + 18.37\, a_B n_{e0}^{1/3}}\right]. \tag{6}$$

2.3 Ion and beam dynamics

The background ions ($j = i$) and the beam ($j = b$) obey the continuity and momentum equations

$$\frac{\partial n_j}{\partial t} + \nabla\cdot\left(n_j \mathbf{v}_j\right) = 0, \tag{7}$$

$$m_i n_j\left(\frac{\partial}{\partial t} + \mathbf{v}_j\cdot\nabla\right)\mathbf{v}_j = Z e n_j\left(-\nabla\phi + \frac{1}{c}\mathbf{v}_j \times \mathbf{B}_0\right) - \gamma k_B T_j \nabla n_j, \tag{8}$$

where $\gamma = 3$ is the adiabatic index for one-dimensional compression. We define the squared thermal speeds $S_j = \gamma k_B T_j/m_i$. The system is closed by Poisson's equation,

$$\nabla^2\phi = 4\pi e(n_e - Z n_i - Z n_b). \tag{9}$$

3. Linear dispersion relation

We linearize Eqs. (2)–(9) about the equilibrium and take perturbations proportional to $\exp(i\mathbf{k}\cdot\mathbf{r} - i\omega t)$. The Doppler-shifted frequency of species j is $\bar{\omega}_j = \omega - k_z v_{j0}$, so that $\bar{\omega}_i = \omega$ and $\bar{\omega}_b = \omega - k_z v_{b0}$.

3.1 Electron response

The Bohm force linearizes to $(\hbar^2/4m_e)\nabla\nabla^2 n_{e1}$ (Haas et al., 2003). The parallel component of Eq. (2) then gives

$$\frac{n_{e1}}{n_{e0}} = \frac{e\phi_1}{m_e V_e^2}, \qquad V_e^2 = C_e^2(1-\alpha_{xc}) + \frac{\hbar^2 k^2}{4m_e^2} \equiv V_{e0}^2 + \frac{\hbar^2 k^2}{4m_e^2}, \tag{10}$$

where V_e is the effective electron response speed. It combines relativistic degeneracy, exchange–correlation (which reduces it) and quantum diffraction (which increases it at short wavelengths).

3.2 Ion and beam response

Introducing the effective potential $\psi_j = Ze\phi_1/m_i + S_j n_{j1}/n_{j0}$ and the ion cyclotron frequency $\Omega_c = ZeB_0/(m_i c)$, the linearized momentum equation becomes $-i\bar{\omega}_j \mathbf{v}_{j1} = -i\mathbf{k}\psi_j + \Omega_c\, \mathbf{v}_{j1}\times\hat{\mathbf{z}}$. Its solution is

$$v_{jx} = \frac{\bar{\omega}_j k_x \psi_j}{\bar{\omega}_j^2 - \Omega_c^2}, \qquad v_{jy} = \frac{-i\,\Omega_c k_x \psi_j}{\bar{\omega}_j^2 - \Omega_c^2}, \qquad v_{jz} = \frac{k_z \psi_j}{\bar{\omega}_j}. \tag{11}$$

The linearized continuity equation gives $n_{j1}/n_{j0} = \mathbf{k}\cdot\mathbf{v}_{j1}/\bar{\omega}_j$. Combining it with Eq. (11) and the definition of ψ_j yields the density response

$$\frac{n_{j1}}{n_{j0}} = \frac{Ze\phi_1}{m_i} \frac{k^2\bar{\omega}_j^2 - k_z^2\Omega_c^2}{\bar{\omega}_j^4 - \bar{\omega}_j^2\left(\Omega_c^2 + k^2 S_j\right) + k_z^2\Omega_c^2 S_j}. \tag{12}$$

For $\Omega_c \to 0$ this reduces to the familiar warm-fluid result $k^2/\left(\bar{\omega}_j^2 - k^2 S_j\right)$.

3.3 Dispersion relation

Substituting Eqs. (10) and (12) into the linearized Poisson equation gives

$$k^2 + \frac{\omega_{pe}^2}{V_e^2} - \sum_{j=i,b} \omega_{pj}^2 \frac{k^2\bar{\omega}_j^2 - k_z^2\Omega_c^2}{\bar{\omega}_j^4 - \bar{\omega}_j^2\left(\Omega_c^2 + k^2 S_j\right) + k_z^2\Omega_c^2 S_j} = 0, \tag{13}$$

where $\omega_{pe}^2 = 4\pi n_{e0}e^2/m_e$ and $\omega_{pj}^2 = 4\pi n_{j0}Z^2e^2/m_i$. The second term represents electron screening, and the sum represents the inertial response of the magnetized, warm background ions and beam.

Dividing Eq. (13) by k^2 gives the dielectric function $\varepsilon = 1 + 1/(k^2\lambda_e^2) + \chi_i + \chi_b$, where $\lambda_e = V_e/\omega_{pe}$ is the quantum–relativistic screening length and χ_j are the ion and beam susceptibilities. In the rest frame of the background plasma, the slow beam mode carries negative wave energy. Instability arises when it coalesces with the positive-energy ion-acoustic mode of the background, which is the standard mechanism of reactive beam–plasma instabilities.

We normalize frequencies by ω_{pi} and lengths by $\lambda = C_q/\omega_{pi}$, where

$$C_q^2 = \frac{Zm_eV_{e0}^2}{m_i} \tag{14}$$

is the quantum–relativistic ion-acoustic speed. The dimensionless parameters are

$$K = k\lambda, \quad W = \frac{\omega}{\omega_{pi}}, \quad U = \frac{v_{b0}}{C_q}, \quad \hat{\Omega} = \frac{\Omega_c}{\omega_{pi}}, \quad \sigma_j = \frac{S_j}{C_q^2}, \quad H = \frac{\hbar\omega_{pi}}{2m_eV_{e0}C_q}, \tag{15}$$

together with $K_z = K\cos\theta$ and $\bar{W} = W - K_zU$. Using Eq. (1), the length unit satisfies $\lambda = \lambda_{e0}\sqrt{1+\delta}$, where $\lambda_{e0} = V_{e0}/\omega_{pe}$, so K essentially measures the wavenumber in units of the electron screening length. With these variables, Eq. (13) becomes

$$\begin{aligned} K^2 + \frac{1+\delta}{1+H^2K^2} - \frac{K^2W^2 - K_z^2\hat{\Omega}^2}{W^4 - W^2\left(\hat{\Omega}^2 + K^2\sigma_i\right) + K_z^2\hat{\Omega}^2\sigma_i} \\ -\delta\,\frac{K^2\bar{W}^2 - K_z^2\hat{\Omega}^2}{\bar{W}^4 - \bar{W}^2\left(\hat{\Omega}^2 + K^2\sigma_b\right) + K_z^2\hat{\Omega}^2\sigma_b} = 0. \end{aligned} \tag{16}$$

Relativistic degeneracy and exchange–correlation enter through C_q, and therefore through U, σ_j, H and $\hat{\Omega}$. Writing the two ion terms as N_j/Q_j and the electron part as $A_e = K^2 + (1+\delta)/(1+H^2K^2)$, Eq. (16) is equivalent to the polynomial equation

$$\mathcal{P}(W) = A_eQ_iQ_b - N_iQ_b - \delta\,N_bQ_i = 0, \tag{17}$$

which is of degree eight in W with real coefficients. Its complex roots occur in conjugate pairs, and the normalized growth rate is

$$\Gamma(K,\theta) = \max \operatorname{Im} W, \qquad \gamma_g = \Gamma\,\omega_{pi}. \tag{18}$$

All algebraic steps from Eq. (2) to Eq. (17) were verified with computer algebra.

4. Analytical limits

4.1 Quantum ion-acoustic and oblique modes

Without a beam ($\delta = 0$) and with unmagnetized ions ($\hat{\Omega} = 0$), Eq. (16) yields the quantum ion-acoustic dispersion relation

$$W^2 = \frac{K^2(1+H^2K^2)}{1+K^2(1+H^2K^2)} + \sigma_iK^2, \tag{19}$$

which for $\sigma_i = 0$ and non-relativistic electrons agrees with Haas et al. (2003). For $K \ll 1$ it gives $\omega = k\sqrt{C_q^2 + S_i}$. With magnetized ions, $\delta = 0$ gives a quadratic in $X = W^2$,

$$A_e X^2 - \left[A_e\left(\hat{\Omega}^2 + K^2\sigma_i\right) + K^2\right]X + K_z^2\hat{\Omega}^2(A_e\sigma_i + 1) = 0, \tag{20}$$

whose roots describe the oblique quantum ion-acoustic mode and an ion-cyclotron-like mode. For $\theta = 0$ these reduce to $W^2 = \hat{\Omega}^2$ and Eq. (19), as for oblique ion-acoustic modes in magnetized quantum plasmas (El-Borie et al., 2020; Sahu et al., 2019). Equation (20) has only real, positive roots, so the plasma is stable without the beam.

4.2 Weak cold beam

For a tenuous ($\delta \ll 1$), cold ($\sigma_b = 0$) beam, instability arises from Cherenkov resonance between the beam and a normal mode W_r of the background, $D_0(W_r) = 0$, where $D_0 = A_e - N_i/Q_i$. The resonance condition is

$$W_r = K_z U = KU\cos\theta. \tag{21}$$

Writing $W = W_r + \Delta$ with $|\Delta| \ll |W_r|$ and expanding $D_0(W) \simeq D_0{}'\Delta$, where $D_0{}' = (\partial D_0/\partial W)_{W_r}$, the beam term becomes $\delta K_{\text{eff}}^2/\Delta^2$. Here $K_{\text{eff}} = K_z$ for a magnetized beam ($|\Delta| \ll \hat{\Omega}$) and $K_{\text{eff}} = K$ for an unmagnetized beam ($|\Delta| \gg \hat{\Omega}$). The resulting cubic $\Delta^3 = \delta K_{\text{eff}}^2/D_0{}'$ has one root with positive imaginary part, giving

$$\Gamma \simeq \frac{\sqrt{3}}{2}\left|\frac{\delta K_{\text{eff}}^2}{D_0{}'}\right|^{1/3}. \tag{22}$$

For unmagnetized, cold background ions, $D_0{}' = 2K^2/W_r^3$, and Eq. (22) becomes

$$\Gamma \simeq \frac{\sqrt{3}}{2}\left(\frac{\delta}{2}\right)^{1/3} W_r, \qquad W_r = \frac{K\sqrt{1 + H^2K^2}}{\sqrt{1 + \delta + K^2(1 + H^2K^2)}}. \tag{23}$$

The $\delta^{1/3}$ scaling is characteristic of a reactive fluid beam instability. The distinction between K_z and K shows that ion magnetization reduces the coupling of an oblique wave to the beam.

5. Numerical results and discussion

5.1 Parameters

Equation (17) was solved with a polynomial root finder (companion-matrix eigenvalues), followed by three Newton iterations on $\mathcal{P}(W)$ to refine each root. Roots at which Q_i or Q_b vanishes are introduced by the multiplication that produced Eq. (17) and were discarded; every retained root satisfies Eq. (16) to within 10^{-6} relative to the size of its individual terms. The growth rate was evaluated on grids of 400 wavenumbers for the two-dimensional curves and of 110×81 or 110×90 points for the three-dimensional surfaces. Growth rates below 10^{-7} were treated as zero, which removes round-off noise without affecting any physical result. The code reproduces Eq. (20) to a relative accuracy of 10^{-12} and Eq. (19) to 10^{-15}, and it returns zero growth for $\delta = 0$. The reference plasma is helium ($Z = 2$, $A = 4$), with the parameters listed in Table 1.

Table 1 - Reference parameters and the derived dimensionless quantities.

Physical parameter	Value	Dimensionless parameter	Value
Electron density n_{e0}	10^{29} cm^{-3}	Relativity parameter R	0.555
Magnetic field B_0	10^{12} G	Exchange–correlation α_{xc}	0.0048
Ion temperature T_i	10^8 K	Magnetization $\hat{\Omega}$	0.0171
Beam temperature T_b	10^7 K	Quantum diffraction H	0.123
Beam density ratio δ	0.1	Ion thermal ratio σ_i	0.284
Beam speed $U = v_{b0}/C_q$	1.6	Beam thermal ratio σ_b	0.028
Ion-acoustic speed C_q	1.48×10^8 cm s^{-1}	ω_{pi}	2.81×10^{17} s^{-1}
Length unit λ	5.26×10^{-10} cm	Electron degeneracy T_e/T_{Fe}	0.12

These parameters satisfy the assumptions of the model. The electrons are degenerate ($T_e/T_{Fe} = 0.12$) and moderately relativistic ($R = 0.555$). The Landau quantization parameter $\hbar\omega_{ce}/\mu_e = 0.020$ is small, so the isotropic Chandrasekhar pressure applies. The ion coupling parameter is 0.40, small enough to justify an ideal ion fluid (Moldabekov et al., 2017; Patidar & Sharma, 2020). Because the wavelength approaches the Fermi wavelength for $K \gtrsim 3$, where QHD loses accuracy (Bonitz et al., 2019; Moldabekov et al., 2018), results are presented for $K \leq 3$.

5.2 Electron equation of state

Figure 1(a) compares C_e from Eq. (4) with its non-relativistic and ultra-relativistic limits. The ratio of the non-relativistic to the relativistic value is $(1 + R^2)^{1/4}$, so the non-relativistic expression overestimates C_e increasingly above $R \approx 0.3$; at $R = 1$ the overestimate is 19% in C_e and 41% in C_e^2. Figure 1(b) shows that exchange–correlation reduces V_{e0}^2 by 4.3% at 10^{26} cm^{-3} but by only 0.48% at 10^{29} cm^{-3} and 0.24% at 10^{32} cm^{-3}. The exchange potential scales as $n_e^{1/3}$, whereas the Fermi energy scales as $n_e^{2/3}$ in the non-relativistic regime and as $n_e^{1/3}$ in the ultra-relativistic one. The ratio therefore falls as $n_e^{-1/3}$ and then levels off at about 0.24%, so exchange–correlation is a small correction at the densities of interest. Exchange–correlation corrections of this kind have been included in earlier QHD studies of ion-acoustic waves (Roy & Sahu, 2020; Shukla & Eliasson, 2012).

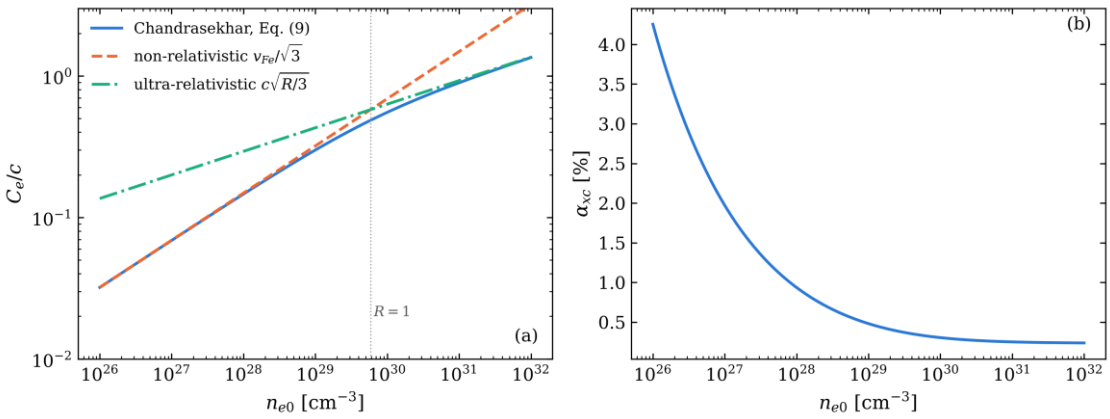


Fig. 1 - (a) Relativistic Fermi sound speed C_e/c from Eq. (4) with its non-relativistic and ultra-relativistic limits. (b) Exchange–correlation parameter α_{xc} of Eq. (6) versus electron density.

5.3 Dispersion characteristics

Figure 2(a) displays the real parts of all roots of Eq. (17) for parallel propagation at the reference parameters. Two beam modes, $W \simeq K\left(U \pm \sqrt{\sigma_b}\right)$, straddle the beam line $W = KU$, and the quantum ion-acoustic branch lies below them. For $K < 0.66$ the slow beam mode and the ion-acoustic mode merge into a complex-conjugate pair (highlighted), which is the signature of a reactive instability. The corresponding growth rate, Fig. 2(b), reaches $\Gamma = 0.0615$ at $K = 0.455$, with $\mathrm{Re}\, W = 0.517$. In physical units this is $\gamma_g = 1.73 \times 10^{16}$ s^{-1}, or an e-folding time of 58 as, at a wavelength of 7.3×10^{-9} cm. These three branches parallel the ion-acoustic and beam-driven modes identified by Elkamash et al. (2017) in the unmagnetized limit.

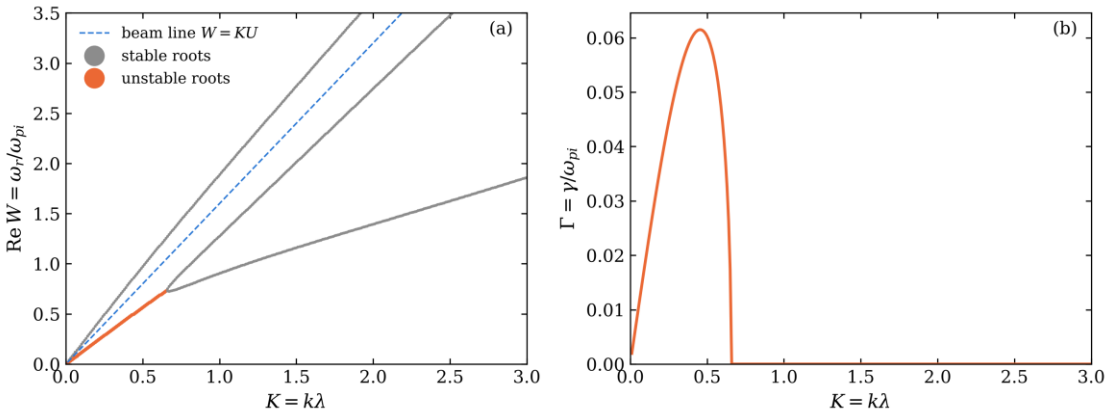


Fig. 2 - (a) Real parts of the roots of Eq. (17) for $\theta = 0$; unstable roots are highlighted. (b) Normalized growth rate. Reference parameters of Table 1.

5.4 Effect of beam density and beam speed

Figure 3 shows that a denser beam strengthens and broadens the instability. As δ increases from 0.05 to 0.3, the peak growth rate rises from 0.0283 to 0.127, and the unstable range extends from $K < 0.44$ to $K < 1.00$. The increase is close to the $\delta^{1/3}$ law of Eq. (22) at small δ and faster at larger δ,

where the beam modifies the background mode itself. The dependence of the growth rate on beam concentration was also examined by Elkamash et al. (2017) for an unmagnetized plasma.

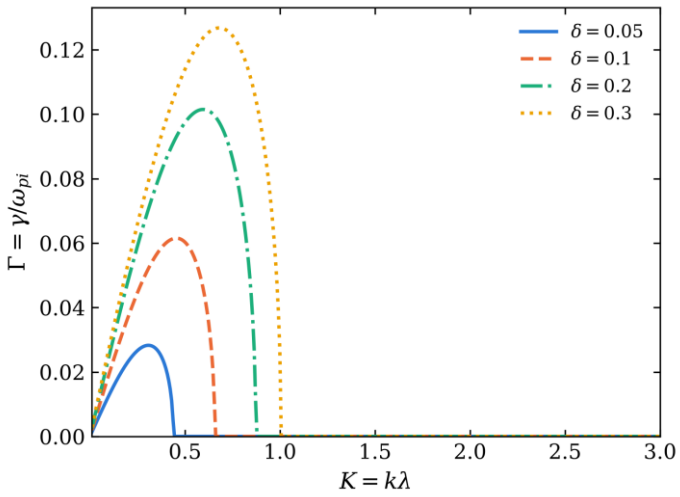


Fig. 3 - Growth rate versus K for four beam density ratios ($\theta = 0$, $U = 1.6$).

The beam speed acts in the opposite direction (Fig. 4). Decreasing U from 1.6 to 0.9 raises the peak growth rate from 0.0615 to 0.161 and shifts it to larger K. This occurs because resonance with the ion-acoustic branch, whose phase speed decreases with K through Eq. (19), then occurs at shorter wavelengths, where the coupling is stronger. The three-dimensional surface of Fig. 5 shows the full dependence. The stability map of Fig. 6 reveals a finite window of unstable beam speeds: for parallel propagation and $\delta = 0.1$, instability requires $0.72 < U < 1.83$. The window widens to $0.71 < U < 2.09$ for $\delta = 0.5$ and narrows to $0.76 < U < 1.50$ for $\delta = 0.01$. The maximum growth rate in the map, 0.267, occurs near $U \approx 1$ for $\delta = 0.5$. A beam that is too fast cannot stay in resonance with the ion-acoustic branch. For a slow beam, the relative drift is too small compared with the ion-acoustic and thermal speeds for the beam and background modes to coalesce.

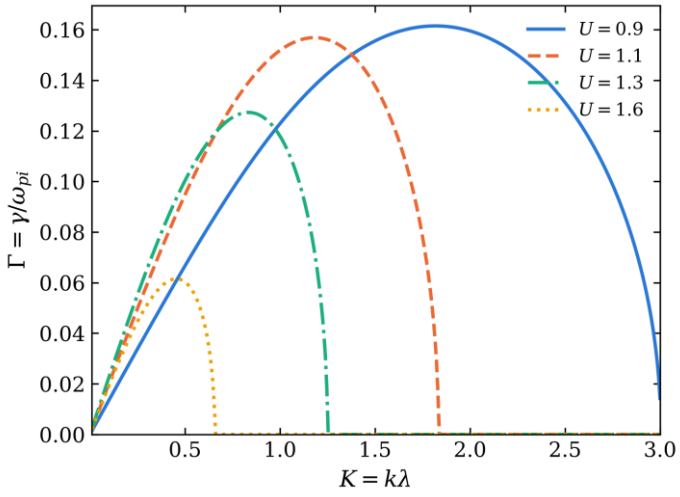


Fig. 4 - Growth rate versus K for four normalized beam speeds ($\theta = 0$, $\delta = 0.1$).

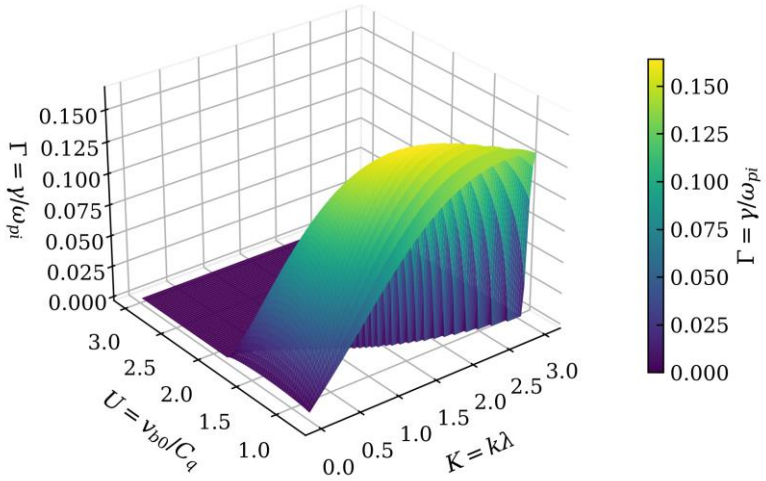


Fig. 5 - Growth rate $\Gamma(K, U)$ for parallel propagation and $\delta = 0.1$.

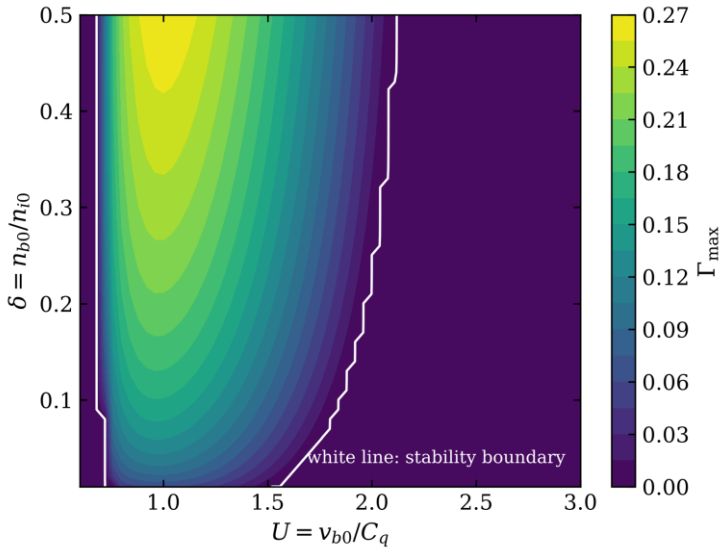


Fig. 6 - Maximum growth rate over $K \leq 3$ in the (U, δ) plane for $\theta = 0$. The white contour marks the stability boundary.

5.5 Effect of propagation angle

Oblique propagation changes the instability substantially (Figs. 7 and 8). Because only the projection $U\cos\theta$ enters the resonance condition, Eq. (21), increasing θ lowers the effective beam speed. A beam that is too fast for parallel resonance can therefore become resonant obliquely. At $U = 1.6$ the peak growth rate rises from 0.0615 at $\theta = 0$ to 0.0847 at 20° and 0.140 at 40°, and the unstable range extends to $K = 1.44$. The global maximum of the surface, $\Gamma = 0.164$, occurs at $\theta \approx 53°$ and $K \approx 1.56$, where $U\cos\theta \approx 0.96$ lies near the most unstable beam speed of Fig. 6. Since $\hat{\Omega} = 0.017$ is small, ion magnetization matters only where the growth rate itself is comparable to or smaller than $\hat{\Omega}$. This occurs at the long-wavelength edge of the spectrum ($K \lesssim 0.2$ for $\theta = 60°$), where the beam responds as a magnetized fluid and $K_{\text{eff}} = K_z$ in Eq. (22). This weak magnetization is consistent with the requirement that the electrons remain non-quantizing. Oblique propagation is likewise known to modify ion-acoustic structures in magnetized degenerate plasmas (El-Borie et al., 2020; Sultana et al., 2019).

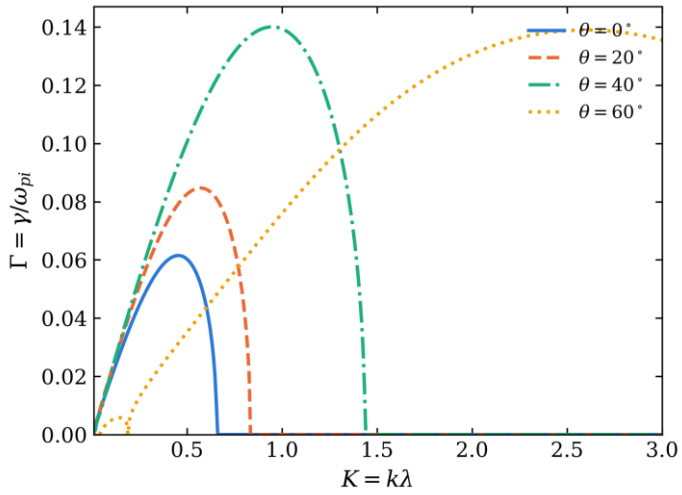


Fig. 7 - Growth rate versus K for four propagation angles ($U = 1.6$, $\delta = 0.1$).

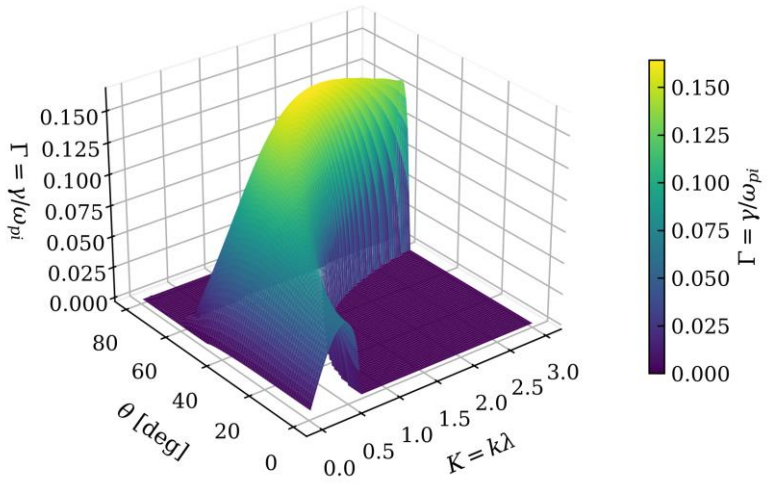


Fig. 8 - Growth rate $\Gamma(K, \theta)$ at the reference parameters.

5.6 Relativistic and quantum effects

To isolate individual physical effects, Fig. 9 compares growth rates at a fixed physical beam speed, $v_{b0} = 2.36 \times 10^8$ cm s^{-1}, in the units of the reference plasma. Relativistic degeneracy is the dominant correction. With the non-relativistic Fermi pressure, the peak growth rate is 0.0826 instead of 0.0615 (34% larger), and the unstable range extends to $K = 0.75$. The non-relativistic model overestimates C_q, which lowers the effective U from 1.60 to 1.50 and moves the beam towards the centre of the unstable window. Exchange–correlation lowers C_q slightly, so removing it raises the peak growth rate by 1.3%. Quantum diffraction raises the growth rate by only 0.9%, because $H^2K^2 \approx 3 \times 10^{-3}$ at the most unstable wavenumber. Exchange–correlation and quantum diffraction have been retained in earlier studies of ion-acoustic waves in dense plasmas (Mahmood et al., 2019; Rajabi & Mohammadnejad, 2023; Shome et al., 2020); for beam-driven growth, the present results show that their combined effect is at the percent level.

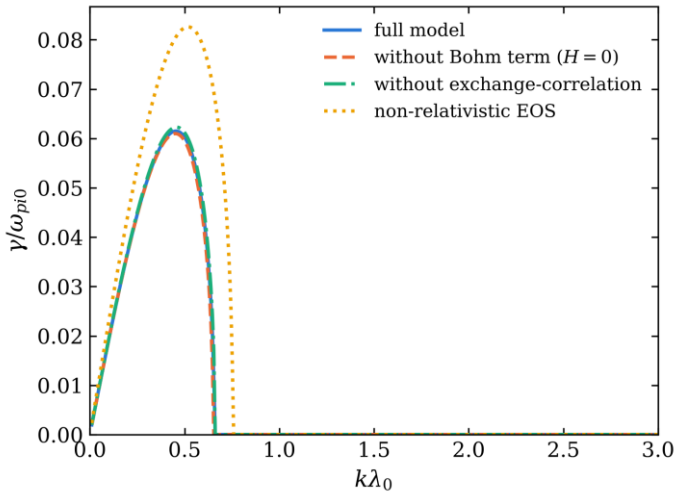


Fig. 9 - Growth rate at fixed physical beam speed for the full model, without the Bohm term, without exchange–correlation, and with the non-relativistic equation of state.

Figure 10 shows the maximum growth rate (over $K \leq 3, \theta = 0$) and the corresponding wavenumber as functions of density at the same fixed beam speed. Instability sets in at $n_{e0} = 5.9 \times 10^{28}$ cm^{-3} for the Chandrasekhar equation of state and at 5.1×10^{28} cm^{-3} for the non-relativistic one. Below these densities C_q is so small that U exceeds the upper edge of the unstable window. Above onset the growth rate rises steeply, to 1.73×10^{16} s^{-1} at 10^{29}, 1.69×10^{17} s^{-1} at 10^{30} and 6.42×10^{17} s^{-1} at 10^{31} cm^{-3}. The non-relativistic model gives larger values at 10^{29} and 10^{30} cm^{-3} (by 34% and 11%). At 10^{31} cm^{-3} it gives a slightly smaller value, because its overestimated C_q drives U to 0.32, below the optimal beam speed. The relativistic softening of the equation of state therefore has a non-monotonic effect on the instability. Figure 11 shows the same dependence as a three-dimensional surface in the units of the reference plasma.

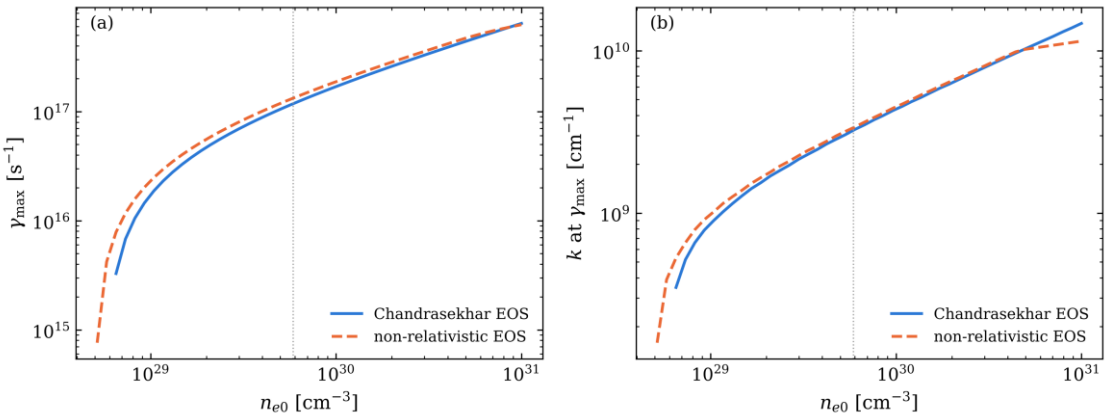


Fig. 10 - (a) Maximum growth rate and (b) wavenumber of maximum growth versus electron density at fixed physical beam speed, for the Chandrasekhar and non-relativistic equations of state. The dotted line marks $R = 1$.

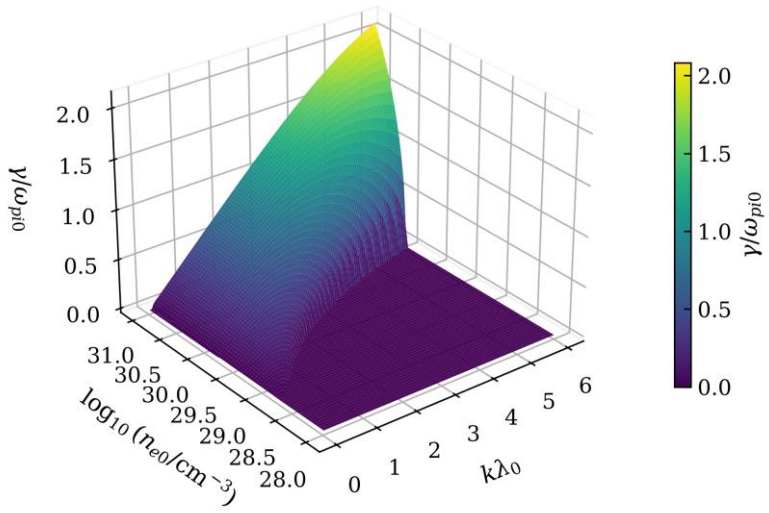


Fig. 11 - Growth rate versus wavenumber and electron density at fixed physical beam speed, in units of the reference plasma.

5.7 Validation of the weak-beam theory

Figure 12 compares exact roots of Eq. (17) with Eq. (23) for a cold, unmagnetized system at $K = 0.6$, with the beam speed set to resonance. The agreement is within 0.9% at $\delta = 10^{-5}$, 4.1% at $\delta = 10^{-3}$ and 9.4% at $\delta = 10^{-2}$. It degrades to 23% at $\delta = 0.1$, where the expansion parameter $|\Delta/W_r|$ is no longer small. The exact results confirm the $\delta^{1/3}$ scaling over four decades of beam density. The same formula with $K_{\mathrm{eff}} = K_z$ reproduces the magnetized oblique growth rate to within 4%.

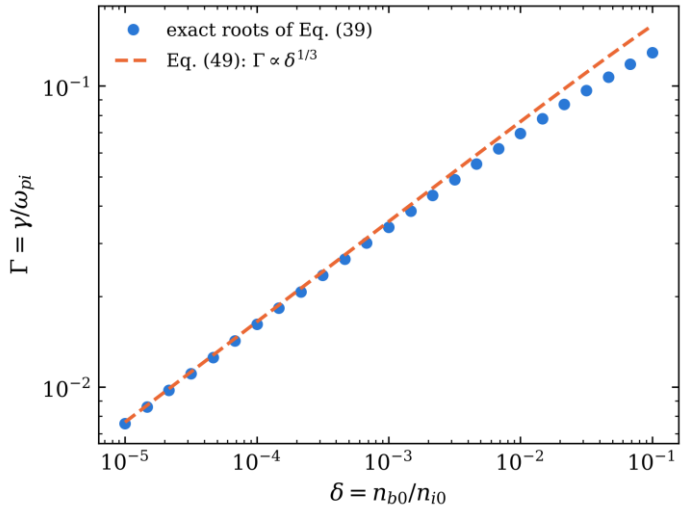


Fig. 12 - Growth rate versus beam density: exact roots of Eq. (17) and the weak-beam formula, Eq. (23).

5.8 Physical implications

The growth rates found here are large. At the reference point the e-folding time, 58 as, equals 2.6 ion plasma periods ($2\pi/\omega_{pi} = 22$ as). A beam carrying 10% of the ion density would therefore excite ion-acoustic fluctuations within a few ion plasma periods. The most unstable wavelength, 7.3×10^{-9} cm, is about 14 times the length unit λ, comfortably within the long-wavelength regime in which QHD applies (Bonitz et al., 2019; Moldabekov et al., 2018).

A second implication concerns fast beams. Because ion magnetization is weak, the growth rate depends on the beam speed essentially through $U\cos\theta$. This is confirmed by the equality of the global maxima of Figs. 5 and 8 ($\Gamma = 0.164$ in both). A beam faster than the parallel stability limit is therefore not stable: it drives waves at the angle for which $U\cos\theta$ falls inside the unstable window. For example, a beam with $U = 5$ produces the same maximum growth rate, $\Gamma = 0.164$, at $\theta = 79°$. Oblique ion-acoustic turbulence is thus the expected outcome of fast ion beams in dense degenerate plasmas, for instance energetic ion populations in compressed fusion targets (Abu-Shawareb et al., 2024; Betti & Hurricane, 2016), provided the propagation remains within the electrostatic and fluid limits discussed above.

5.9 Limitations

The model neglects kinetic ion Landau damping, which is weak only when the phase speed greatly exceeds the ion thermal speed; at the reference point $\sigma_i = 0.28$, so some reduction of the fluid growth rates is expected. Kinetic and fluid descriptions of relativistic ion-acoustic waves can also differ quantitatively (Haas, 2016). Ion–ion correlations, important for coupling parameters above unity (Moldabekov et al., 2017; Patidar & Sharma, 2020), are also omitted. The Bohm term uses the electron rest mass, and the exchange–correlation potential is non-relativistic; both are small corrections here. Electron inertia is neglected, which excludes the high-frequency electron-plasma branch found by Elkamash et al. (2017). Finally, the electrostatic approximation neglects coupling to magnetosonic and Alfvén waves, which may introduce corrections of order $\left(v_{ph}/V_A\right)^2 \approx 0.1$ at the reference parameters.

6. Conclusions

The linear stability of a field-aligned ion beam in a magnetized, relativistically degenerate plasma has been analysed with a three-fluid QHD model that includes the Chandrasekhar pressure, quantum diffraction, exchange–correlation and warm, magnetized ions and beam. The exact dispersion relation reduces to a degree-eight polynomial, Eq. (17), whose roots give the growth rate for arbitrary propagation angle. For a weak cold beam, $\Gamma \propto \delta^{1/3}$, with the field-aligned wavenumber governing a magnetized beam and the full wavenumber an unmagnetized one, Eq. (22). For parallel propagation the instability exists only within a window of beam speeds, $0.72 < U < 1.83$ for $\delta = 0.1$. Oblique propagation shifts the effective speed into this window, giving a maximum growth rate of $0.164\,\omega_{pi}$ at $\theta \approx 53^\circ$. Relativistic degeneracy is the dominant correction. The non-relativistic Fermi pressure overestimates the growth rate by 34% at $10^{29}\,\mathrm{cm}^{-3}$, and the effect becomes non-monotonic at higher density. Exchange–correlation and quantum diffraction change the growth rate by about 1% within the validity range of the fluid model. These results identify the beam speed relative to the quantum–relativistic ion-acoustic speed, and the propagation angle, as the key parameters controlling beam-driven instabilities in dense stellar and laboratory plasmas (Abu-Shawareb et al., 2024; Ferrario et al., 2020). Kinetic damping, ion correlations, electron inertia and electromagnetic coupling should be included in future work. Particle-in-cell or quantum kinetic simulations of the nonlinear stage would also clarify how the oblique ion-acoustic fluctuations predicted here saturate and how efficiently they heat the background ions.

Author contributions

Ahsan Iqbal: conceptualization, methodology, formal analysis, software, writin original draft. Muhammad Rizwan: validation, writing – review and editing. Shahnaz Maryam: visualization.

Conflict of interest

The authors declare no conflict of interest.

Data availability statement

The data supporting the findings of this study were generated with the Python code described in Section 5 and are available from the corresponding author on reasonable request.

References

Abdikian, A. (2017). Modulational instability of ion-acoustic waves in magnetoplasma with pressure of relativistic electrons. *Physics of Plasmas*, *24*(5), 052123. https://doi.org/10.1063/1.4984247

Abu-Shawareb, H., Acree, R., Adams, P., Adams, J., Addis, B., Aden, R., Adrian, P., Afeyan, B. B., Aggleton, M., Aghaian, L., Aguirre, A., Aikens, D., Akre, J., Albert, F., Albrecht, M., Albright, B. J., Albritton, J., Alcala, J., Alday, C., . . . The Indirect Drive ICF Collaboration (2024). Achievement of target gain larger than unity in an inertial fusion experiment. *Physical Review Letters*, *132*(6), 065102. https://doi.org/10.1103/PhysRevLett.132.065102

Atteya, A., Behery, E. E., & El-Taibany, W. F. (2017). Ion acoustic shock waves in a degenerate relativistic plasma with nuclei of heavy elements. *The European Physical Journal Plus*, *132*(3), 109. https://doi.org/10.1140/epjp/i2017-11367-2

Behery, E. E., Haas, F., & Kourakis, I. (2016). Weakly nonlinear ion-acoustic excitations in a relativistic model for dense quantum plasma. *Physical Review E*, *93*(2), 023206. https://doi.org/10.1103/physreve.93.023206

Betti, R., & Hurricane, O. A. (2016). Inertial-confinement fusion with lasers. *Nature Physics*, *12*(5), 435–448. https://doi.org/10.1038/nphys3736

Bonitz, M., Moldabekov, Zh. A., & Ramazanov, T. S. (2019). Quantum hydrodynamics for plasmas—Quo vadis? *Physics of Plasmas*, *26*(9), 090601. https://doi.org/10.1063/1.5097885

Bret, A. (2021). Quantum electrodynamic effects on the two-stream instability. *EPL (Europhysics Letters)*, *135*(3), 35001. https://doi.org/10.1209/0295-5075/ac1e44

Brey, L., Dempsey, J., Johnson, N. F., & Halperin, B. I. (1990). Infrared optical absorption in imperfect parabolic quantum wells. *Physical Review B*, *42*(2), 1240–1247. https://doi.org/10.1103/PhysRevB.42.1240

Chandrasekhar, S. (1935). The highly collapsed configurations of a stellar mass. (Second paper.). *Monthly Notices of the Royal Astronomical Society*, *95*(3), 207–225. https://doi.org/10.1093/mnras/95.3.207

Deka, M. K., & Dev, A. N. (2018). Landau degeneracy effect on ion beam driven degenerate magneto plasma: Evolution of hypersonic soliton. *Annals of Physics*, *395*, 45–62. https://doi.org/10.1016/j.aop.2018.05.008

Deka, M. Kr., Dev, A. N., Misra, A. P., & Adhikary, N. C. (2018). Characteristics of solitary waves in a relativistic degenerate ion beam driven magneto plasma. *Physics of Plasmas*, *25*(1), 012102. https://doi.org/10.1063/1.5004070

Dornheim, T., Groth, S., & Bonitz, M. (2018). The uniform electron gas at warm dense matter conditions. *Physics Reports*, *744*, 1–86. https://doi.org/10.1016/j.physrep.2018.04.001

El-Borie, M. A., Abd-Elzaher, M., & Atteya, A. (2020). Obliquely propagating ion-acoustic solitary and shock waves in magnetized quantum degenerate multi-ions plasma in the presence of trapped electrons. *Chinese Journal of Physics*, *63*, 258–270. https://doi.org/10.1016/j.cjph.2019.10.004

Elkamash, I. S., Haas, F., & Kourakis, I. (2017). Ion-beam/plasma modes in ultradense relativistic quantum plasmas: Dispersion characteristics and beam-driven instability. *Physics of Plasmas*, *24*(9), 092119. https://doi.org/10.1063/1.4989777

Ferrario, L., Wickramasinghe, D., & Kawka, A. (2020). Magnetic fields in isolated and interacting white dwarfs. *Advances in Space Research*, *66*(5), 1025–1056. https://doi.org/10.1016/j.asr.2019.11.012

Ghai, Y., Saini, N. S., & Eliasson, B. (2019). Neutrino-driven instability of ion acoustic waves in an ultrarelativistic degenerate plasma. *The Astrophysical Journal*, *884*(1), 27. https://doi.org/10.3847/1538-4357/ab3e0c

Gul, N., & Ahmad, R. (2021). Modulation instability of ion-acoustic waves and exchange interaction in magnetized quantum plasma with relative density effects of spin-up and spin-down electrons. *Physica Scripta*, *96*(5), 055602. https://doi.org/10.1088/1402-4896/abe679

Haas, F. (2016). Modelling of relativistic ion-acoustic waves in ultra-degenerate plasmas. *Journal of Plasma Physics*, *82*(6), 705820602. https://doi.org/10.1017/s0022377816001100

Haas, F., & Mahmood, S. (2016). Nonlinear ion-acoustic solitons in a magnetized quantum plasma with arbitrary degeneracy of electrons. *Physical Review E*, *94*(3), 033212. https://doi.org/10.1103/PhysRevE.94.033212

Haas, F., Garcia, L. G., Goedert, J., & Manfredi, G. (2003). Quantum ion-acoustic waves. *Physics of Plasmas*, *10*(10), 3858–3866. https://doi.org/10.1063/1.1609446

Kaur, R., & Saini, N. S. (2021). Ion acoustic shocks in a weakly relativistic ion-beam degenerate magnetoplasma. *Galaxies*, *9*(3), 64. https://doi.org/10.3390/galaxies9030064

Khanum, U., Iqbal, Z., & Murtaza, G. (2020). Hydrodynamic analysis of electrostatic counter-streaming instability in a spin-polarized electron–positron–ion plasma. *Contributions to Plasma Physics*, *60*(9), e202000024. https://doi.org/10.1002/ctpp.202000024

Lee, M.-J., & Jung, Y.-D. (2018). Resonant streaming instability in a non-degenerate quantum plasma including the electron quantum recoil effect. *Physics of Plasmas*, *25*(9), 092109. https://doi.org/10.1063/1.5046953

Madhukalya, B., Das, R., Hosseini, K., Baleanu, D., & Salahshour, S. (2023). Small amplitude ion-acoustic solitary waves in a magnetized ion-beam plasma under the effect of ion and beam temperatures. *The European Physical Journal Plus*, *138*(4), 315. https://doi.org/10.1140/epjp/s13360-023-03897-3

Mahmood, S., Ur-Rehman, H., Hussain, S., & Adnan, M. (2019). Nonlinear excitation and stability analysis of ion-acoustic waves in a magnetized quantum plasma with exchange-correlation effects of degenerate electrons. *Physics Letters A*, *383*(26), 125840. https://doi.org/10.1016/j.physleta.2019.125840

Manfredi, G., & Haas, F. (2001). Self-consistent fluid model for a quantum electron gas. *Physical Review B*, *64*(7), 075316. https://doi.org/10.1103/PhysRevB.64.075316

McKerr, M., Haas, F., & Kourakis, I. (2016). Ion-acoustic envelope modes in a degenerate relativistic electron-ion plasma. *Physics of Plasmas*, *23*(5), 052120. https://doi.org/10.1063/1.4952774

Moldabekov, Zh. A., Bonitz, M., & Ramazanov, T. S. (2018). Theoretical foundations of quantum hydrodynamics for plasmas. *Physics of Plasmas*, *25*(3), 031903. https://doi.org/10.1063/1.5003910

Moldabekov, Zh. A., Groth, S., Dornheim, T., Bonitz, M., & Ramazanov, T. S. (2017). Ion potential in non-ideal dense quantum plasmas. *Contributions to Plasma Physics*, *57*(10), 532–538. https://doi.org/10.1002/ctpp.201700109

Patidar, A., & Sharma, P. (2020). Ion acoustic solitary and shock waves in strongly coupled degenerate plasma with relativistic effects. *Physica Scripta*, *95*(8), 085603. https://doi.org/10.1088/1402-4896/ab9be0

Rajabi, B., & Mohammadnejad, M. (2023). Modulational instability of ion-acoustic waves in a dense quantum plasma. *Physics of Plasmas*, *30*(8), 082112. https://doi.org/10.1063/5.0154769

Roy, D., & Sahu, B. (2020). Electron-exchange potential correction on dynamics of multidimensional ion acoustic waves in quantum plasmas. *Physics of Plasmas*, *27*(6), 062305. https://doi.org/10.1063/1.5144761

Sahu, B., Sinha, A., & Roychoudhury, R. (2019). Ion-acoustic waves in dense magneto-rotating quantum plasma. *Physics of Plasmas*, *26*(7), 072119. https://doi.org/10.1063/1.5082868

Schreiber, M. R., Belloni, D., Zorotovic, M., Zapata, S., Gänsicke, B. T., & Parsons, S. G. (2022). Magnetic dynamos in white dwarfs – III. Explaining the occurrence of strong magnetic fields in close double white dwarfs. *Monthly Notices of the Royal Astronomical Society*, *513*(2), 3090–3103. https://doi.org/10.1093/mnras/stac1076

Shome, P., Sahu, B., & Poria, S. (2020). Nonlinear dynamics of ion-acoustic waves in quantum plasmas with exchange-correlation effects. *Zeitschrift für Naturforschung A*, *75*(8), 677–685. https://doi.org/10.1515/zna-2020-0008

Shukla, P. K., & Eliasson, B. (2011). Colloquium: Nonlinear collective interactions in quantum plasmas with degenerate electron fluids. *Reviews of Modern Physics*, *83*(3), 885–906. https://doi.org/10.1103/RevModPhys.83.885

Shukla, P. K., & Eliasson, B. (2012). Novel attractive force between ions in quantum plasmas. *Physical Review Letters*, *108*(16), 165007. https://doi.org/10.1103/PhysRevLett.108.165007

Singh, S. S., Jyoti, & Misra, K. P. (2022). Two stream instabilities in unmagnetized nonrelativistic quantum plasma. *Plasma Research Express*, *4*(2), 025006. https://doi.org/10.1088/2516-1067/ac73e5

Sultana, S., & Schlickeiser, R. (2018). Arbitrary amplitude nucleus-acoustic solitons in multi-ion quantum plasmas with relativistically degenerate electrons. *Physics of Plasmas*, *25*(2), 022110. https://doi.org/10.1063/1.5023302

Sultana, S., Islam, S., Mamun, A. A., & Schlickeiser, R. (2019). Oblique propagation of ion-acoustic solitary waves in a magnetized plasma with electrons following a generalized distribution function. *Physics of Plasmas*, *26*(1), 012107. https://doi.org/10.1063/1.5059364